Chemical Engineering Journal 474 (2023) 145516

Contents lists available at ScienceDirect

Chemical Engineering Journal

journal homepage: www.elsevier.com/locate/cej

Synergization of an endoplasmic reticulum-targeted iridium(III) photosensitizer with PD-L1 inhibitor for oral squamous cell carcinoma immunotherapy

Jia-Ying Zhou [a,b,1], Qing-Hua Shen [c,1], Xiao-Jing Hong [a,b,1], Wu-Ya Zhang [a,b], Qiao Su [d], Wu-Guo Li [d], Bin Cheng [a,b,*], Cai-Ping Tan [c,*], Tong Wu [a,b,*]

[a] Hospital of Stomatology, Guanghua School of Stomatology, Sun Yat-sen University, Guangzhou 510055, PR China
[b] Guangdong Provincial Key Laboratory of Stomatology, Guangzhou 510080, PR China
[c] MOE Key Laboratory of Bioinorganic and Synthetic Chemistry, School of Chemistry, Sun Yat-sen University, Guangzhou 510006, PR China
[d] Animal Experiment Center, The First Affiliated Hospital, Sun Yat-sen University, Guangzhou 510080, PR China

ARTICLE INFO

Keywords:
Iridium
Endoplasmic reticulum
Immunogenic cell death
Immune checkpoint inhibitors
Immunotherapy
Oral squamous cell carcinoma

ABSTRACT

Inefficient activation of tumor immunogenicity and sustained immunosuppressive microenvironments severely impede the clinical application of photodynamic therapy (PDT) in oral squamous cell carcinoma (OSCC). Herein, two type I/II iridium(III) photosensitizers (**Ir1** and **Ir2**) targeting endoplasmic reticulum (ER) are designed as immunogenic cell death (ICD) inducers. **Ir1**-meidated PDT treatment adaptively upregulates the programmed death-ligand 1 (PD-L1) expression *in vitro*. Moreover, **Ir1**-mediated PDT stimulates dendritic cell maturation, T lymphocyte infiltration and antitumor cytokine secretion, and synergizes with PD-L1 inhibitor to transform immune-suppressive "cold tumor" to immune-responsive "hot tumor" *in vivo*. Our study firstly paves the way for the combination of metal-based photosensitizing ICD inducer with PD-L1 inhibitor for enhanced immunotherapy.

1. Introduction

Photodynamic therapy (PDT) is an effective modality for cancer therapy due to its noninvasiveness, spatiotemporal precision and high controllability [1]. Besides direct cytotoxicity, PDT can also induce immunogenic cell death (ICD) of tumor cells to promote antitumor immunity [2]. ICD can trigger damage-associated molecular patterns (DAMPs) of tumor cells, subsequently induce the maturation of dendritic cells (DCs) and therefore activate the systemic antitumor immune responses [3,4]. Although cisplatin and oxaliplatin remain the classical chemotherapy agents for many types of cancer including oral squamous cell carcinoma (OSCC), researches indicate that they both fail to induce robust ICD [5,6]. Metal-based photosensitizers (PSs) have revealed significant potential as novel anticancer therapeutic agents [7,8]. Significantly, ruthenium and iridium complexes have been proven to be efficient ICD inducers [9–11]. Especially, by exquisite structural modifications, iridium complexes show interesting PDT properties including specific subcellular targeting, high photo-stability, efficient reactive oxygen species (ROS) production through both type I/II pathway and even oxidation of biomolecules [12–16].

Endoplasmic reticulum (ER) is responsible for crucial biosynthesis, sensing and signaling functions in eukaryotic cells [17]. Therefore, selective disruption of ER function in cancer cells is a promising strategy for anticancer therapy [18]. Especially, ER-targeting chemotherapeutic agents and PSs are proved to be potent ICD inducers by destroying ER protein-folding capacity leading to excessive or aberrant ER stress [19,20]. Recent studies show that metal complexes are promising organelle-targeting ICD-inducing PSs for antitumor immunotherapy in melanoma, breast cancer and hepatocellular carcinoma [21–23].

Notably, ICD inducer monotherapy fails to confer sufficient benefit in many cases, because tumor cells may adaptively upregulate programmed death-ligand 1 (PD-L1) expression to evoke tumor self-protective mechanism after treatment, which further aggravates the immunosuppressive tumor microenvironment (TME) and impedes infiltration and activation of effector T cells [24,25]. Immune checkpoint inhibitors (ICIs) involving programmed death protein 1 (PD-1)

* Corresponding authors at: Hospital of Stomatology, Guanghua School of Stomatology, Sun Yat-sen University, Guangzhou 510055, PR China (Bin Cheng, Tong Wu); MOE Key Laboratory of Bioinorganic and Synthetic Chemistry, School of Chemistry, Sun Yat-sen University, Guangzhou 510006, PR China (Cai-Ping Tan).
E-mail addresses: chengbin@mail.sysu.edu.cn (B. Cheng), tancaip@mail.sysu.edu.cn (C.-P. Tan), wutong23@mail.sysu.edu.cn (T. Wu).
[1] These authors contributed equally to this work.

https://doi.org/10.1016/j.cej.2023.145516
Received 27 May 2023; Received in revised form 21 July 2023; Accepted 16 August 2023
Available online 17 August 2023

and PD-L1 have received extensive attention due to their regulatory function between T cells and tumor cells [26]. However, the responsiveness of PD-1/PD-L1 blockade monotherapy only ranged from 13% to 18% in OSCC [27,28]. ICIs monotherapy provokes unsatisfactory antitumor effects in most patients. The main reason is that the majority of cancer patients have "cold tumors" with defect of antigen presentation, absence of T cell infiltration and activation that do not respond to existing immunotherapeutic agents [29,30]. Besides, PD-L1 inhibitors are only effective for PD-L1 positive patients, while the expression of PD-L1 varies between individuals [31,32]. Therefore, simultaneously increasing immunogenicity by ICD inducers and relieving immunosuppression *via* ICIs are promising strategies to reverse TME from immunosuppressive "cold" to immunogenic "hot" to elicit efficient immune responses. Recent clinical studies have demonstrated an enhanced therapeutic response as well as long-term protection of individuals upon co-treatment with the carboplatin and pembrolizumab or co-treatment with the cisplatin and nivolumab [33–35], which highlights the promising synergistic potential of the combination treatment. Although, there is a possibility to develop a paradigm combining metal-based ICD inducers with ICIs for enhanced cancer photoimmunotherapy, the correlation and synergistic mechanisms between the two treatment methods are not yet clear.

Herein, we designed two cyclometalated iridium(III) complexes (**Ir1** and **Ir2**) with a phenanthroline ligand modified with a hydrophobic long-chain N-phenethylsuccinamide moiety as potent ER-targeted type I/II PSs. **Ir1** selectively accumulates in ER by interacting with the phospholipids and proteins, induces ROS generation through both type I/II PDT pathways and elicits ER stress under visible light (425 nm) irradiation. Meanwhile, **Ir1** leads to release of DAMPs to induce ICD for enhanced tumor immunogenicity, while in parallel **Ir1** upregulates the expression of PD-L1 in OSCC cells. Moreover, cell-derived xenograft (CDX) and oral experimental carcinogenesis models demonstrate that **Ir1**-mediated PDT synergizing PD-L1 immunotherapy elicits robust immune responses through the infiltration of DCs and T lymphocytes, the secretion of antitumor cytokines and the attenuation of immunosuppressive TME, which converts the immune "cold tumor" into "hot

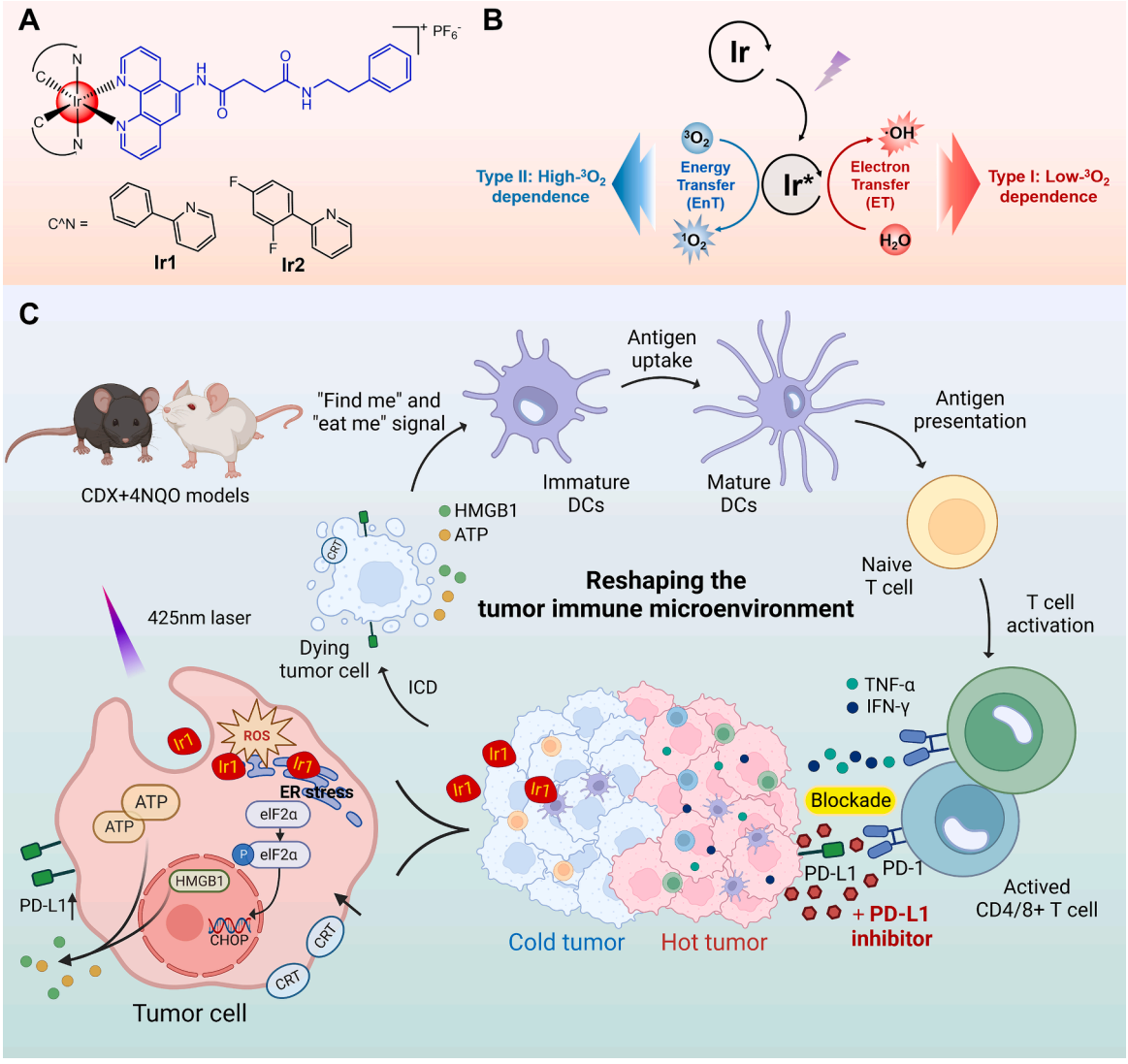

Scheme 1. (A) Chemical structures of **Ir1** and **Ir2**. (B) Schematic diagram of **Ir1** and **Ir2** as type I/II PSs. (C) **Ir1**-mediated PDT evokes ROS-induced ER stress, and releases DAMPs to cause ICD for enhanced tumor immunogenicity. Moreover, PDT acts synergistically in combination with the PD-L1 inhibitor to promote the antigen presentation of DCs, infiltration of T lymphocytes, secretion of antitumor cytokines and response to ICIs therapy, thereby converting the "cold tumor" into "hot tumor" to elicit potent antitumor immune responses. CDX: cell-derived xenograft; 4NQO: 4-nitroquinoline-1-oxide; ROS: reactive oxygen species; ER: endoplasmic reticulum; eIF2α: eukaryotic initiation factor 2 alpha; CHOP: C/EBP homologous protein; CRT: calreticulin; ATP: adenosine triphosphate; HMGB1: high mobility group box-1 protein; PD-1: programmed death protein 1; PD-L1: programmed death ligand 1; ICD: immunogenic cell death; DCs: dendritic cells; TNF-α: tumor necrosis factor-α; IFN-γ: interferon-γ.

tumor" (Scheme 1). As far as we know, it is the first report on the exploration of the synergetic immunomodulatory properties of metal-based ICD PSs and PD-L1 inhibitor, which paves the way for the future clinical transformation of the metal-based PSs for photo-immunotherapy in OSCC.

2. Results and discussion

2.1. Synthesis and characterization

Ir1 and **Ir2** were synthesized by reacting the precursor $[Ir(N–N)_2Cl]_2$ (C^N = 2-phenylpyridine (ppy; **Ir1**); 2-(2,4-difluorophenyl)pyridine (dfppy; **Ir2**)) with the N^1-(1,10-phenanthrolin-5-yl)-N^4-phenethylsuccinamide (**L**) and purified by silica chromatography (Scheme S1). **Ir1** and **Ir2** were characterized by ^{1}H NMR, ^{13}C NMR, ^{19}F NMR, ESI-MS and HPLC (Figs. S1–S11). The absorption spectra of **Ir1** and **Ir2** feature high-energy bands (<350 nm; ligand-centered (^{1}LC) π–π* transitions) and relatively low-energy bands (mixed metal-to-ligand charge-transfer (MLCT) and ligand-to-ligand charge-transfer (LLCT) transitions; Fig. 1A and Fig. S12). **Ir1** and **Ir2** exhibit orange-red phosphorescent emissions upon excitation at 405 nm (Fig. 1A and Fig. S12). Considering the superficial site of OSCC, the 425 nm laser is selected to irradiate iridium complexes to perform PDT. The emission quantum yields of **Ir1** and **Ir2** in PBS, CH_3CN and CH_2Cl_2 fall in the range between 0.019 and 0.146 (Table S1).

The photocatalytic degradation of 9,10-anthracenediyl-bis(methylene)-dimalonic acid (ABDA, $^1O_2$ probe) by **Ir1** and **Ir2** in the presence of light was evaluated in PBS. Using $[Ru(bpy)_3]Cl_2$ (0.18) as the standard, the $^1O_2$ quantum yield of **Ir1** and **Ir2** are calculated to be 0.12 and 0.06, respectively, indicating that **Ir1** has a stronger ability to induce $^1O_2$ (Fig. 1B). Electron spin resonance (ESR) using 2,2,6,6-tetramethyl-4-piperidone (TEMP) as the trapping agent proves the photosensitizing generation of $^1O_2$ by **Ir1** and **Ir2** (Fig. 1C and Fig. S13). Moreover, ESR measurement using 5,5-dimethylpyrroline N-oxide (DMPO) as the trapping agent confirms the production of •OH by **Ir1** and **Ir2** in the presence of light (Fig. 1D and Fig. S14). Moreover, detection of •OH by hydroxyphenyl fluorescein (HPF) further confirms the photosensitizing generation of •OH by **Ir1** and **Ir2** (Fig. S15). These results collectively show that the ROS ($^1O_2$ and •OH) generation capacity of **Ir1** is higher than that of **Ir2**.

To gain insight into the geometric and electronic properties of **Ir1** and **Ir2**, density-functional theory (DFT) and time-dependent density-functional theory (TDDFT) calculations were performed at the PBE1PBE/6-31G*//LanL2DZ level. The highest occupied molecular orbital (HOMO) and the lowest unoccupied molecular orbital (LUMO) energy levels of **Ir1** are −6.26 eV and −2.61 eV, respectively, and the gap of HOMO-LUMO of **Ir1** is 3.65 eV (Fig. 1E). The energy gap between the singlet state and triplet state (ΔE_{s-t}) of **Ir1** is 0.29 eV (Fig. 1F). The HOMO and LUMO of **Ir2** are −6.56 eV and −2.71 eV, respectively. The gap of HOMO-LUMO is 3.85 eV, and the ΔE_{s-t} of **Ir2** is 0.37 eV (Fig. S16). The higher capability of **Ir1** as a type I and type II PDT agent can be explained by its smaller ΔE_{s-t} and better electron-donating ability, which is important for the production of •OH [36,37].

2.2. Ir1 exerts potent photocytotoxicity in vitro

The photocytotoxicity effects of **Ir1** and **Ir2** *in vitro* were evaluated on human OSCC (CAL33, HSC6 and SCC1) and dysplasia oral keratinocyte (DOK) cell lines by Cell Counting Kit-8 (CCK-8) assay (Table 1 and Table S2). **Ir1** and **Ir2** show a lower dark cytotoxicity than cisplatin

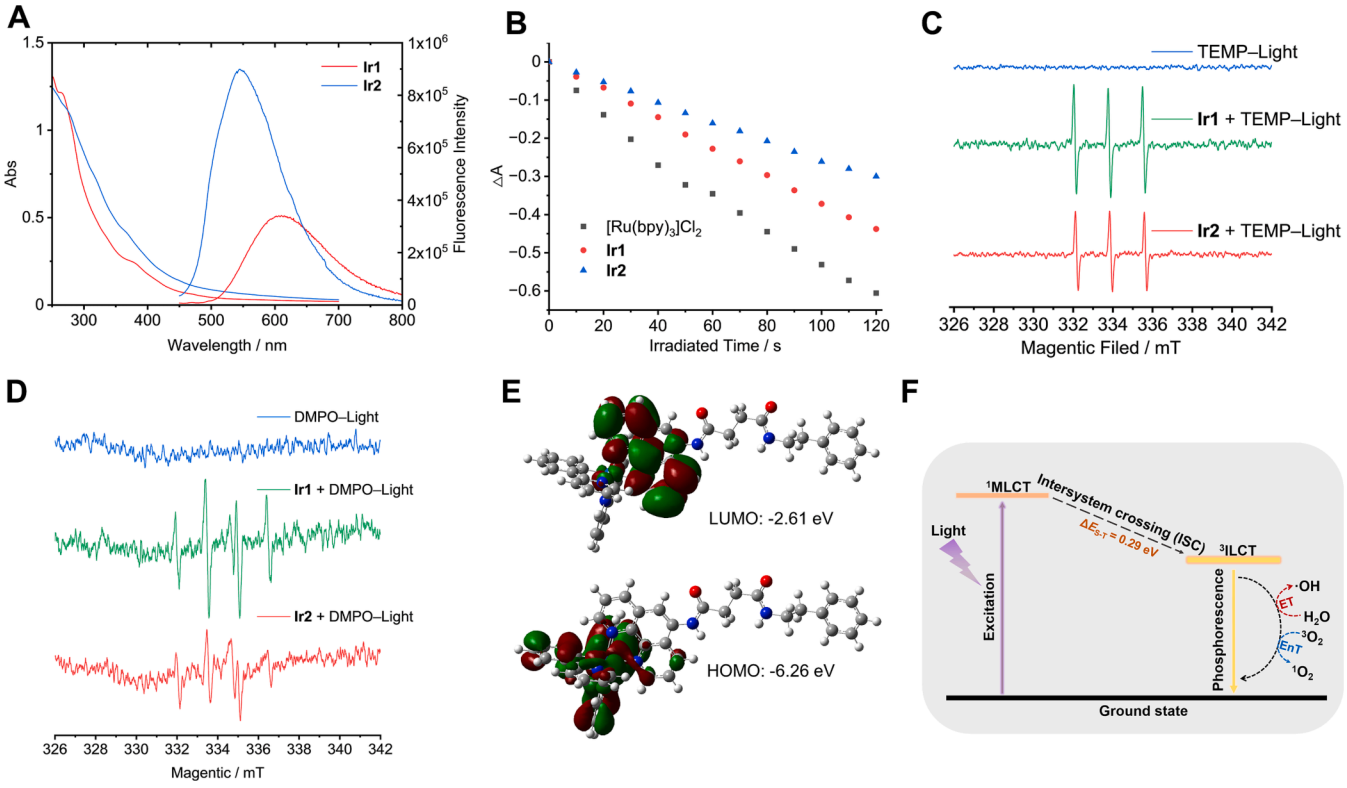

Fig. 1. **Ir1** and **Ir2** can generate $^1O_2$ and •OH in the presence of light. (A) UV–Vis absorption spectra and emission spectra (λ_{ex} = 405 nm) of **Ir1** and **Ir2** (20 μM) in PBS. (B) The capability of **Ir1** and **Ir2** to photosensitize the generation of $^1O_2$ using ABDA as the probe and $[Ru(bpy)_3]Cl_2$ as the standard. The solutions were irradiated with a 425 nm laser (20 mW cm^{-2}) for different time intervals. (C) The ESR spectra of $^1O_2$ generated by **Ir1**/**Ir2** (100 μM) in the presence of light (20 mW cm^{-2}, 3 min) using TEMP (10 mM) as the trapping agent. (D) The ESR spectra of •OH generated by **Ir1**/**Ir2** (100 μM) in the presence of light (20 mW cm^{-2}, 5 min) using DMPO (100 mM) as the trapping agent. (E) HOMO and LUMO of **Ir1**. (F) The mechanisms of **Ir1** to generate ROS through both type I/II pathways. ILCT: intraligand charge-transfer.

Table 1
Cytotoxicity (IC_{50}, μM) of the tested compounds on OSCC cell lines.

Compounds	CAL33			HSC6			SCC1		
	Dark	Light	PI	Dark	Light	PI	Dark	Light	PI
Ir1	19.90 ± 1.83	0.66 ± 0.13	30.34	33.40 ± 2.31	0.68 ± 0.02	48.80	14.00 ± 1.41	0.12 ± 0.05	120.43
Ir2	15.94 ± 0.63	1.06 ± 0.19	15.10	27.34 ± 4.08	1.05 ± 0.02	26.02	13.23 ± 1.51	0.30 ± 0.01	43.66
Cisplatin	4.36 ± 1.59	3.00 ± 0.38	1.45	8.08 ± 0.14	3.67 ± 0.07	2.20	9.03 ± 0.88	10.93 ± 2.38	0.83

IC_{50} value is the drug concentration necessary for 50% inhibition of cell viability. Cells were incubated with the tested compounds for 48 h and detected by CCK-8 assay in the absence and presence of 425 nm light (20 mW cm^{-2}, 15 min). Phototoxicity index (PI) is defined as the ratio of $^{dark}IC_{50}/^{light}IC_{50}$. Data are presented as the means ± standard deviations (SD) of three repeated measurements.

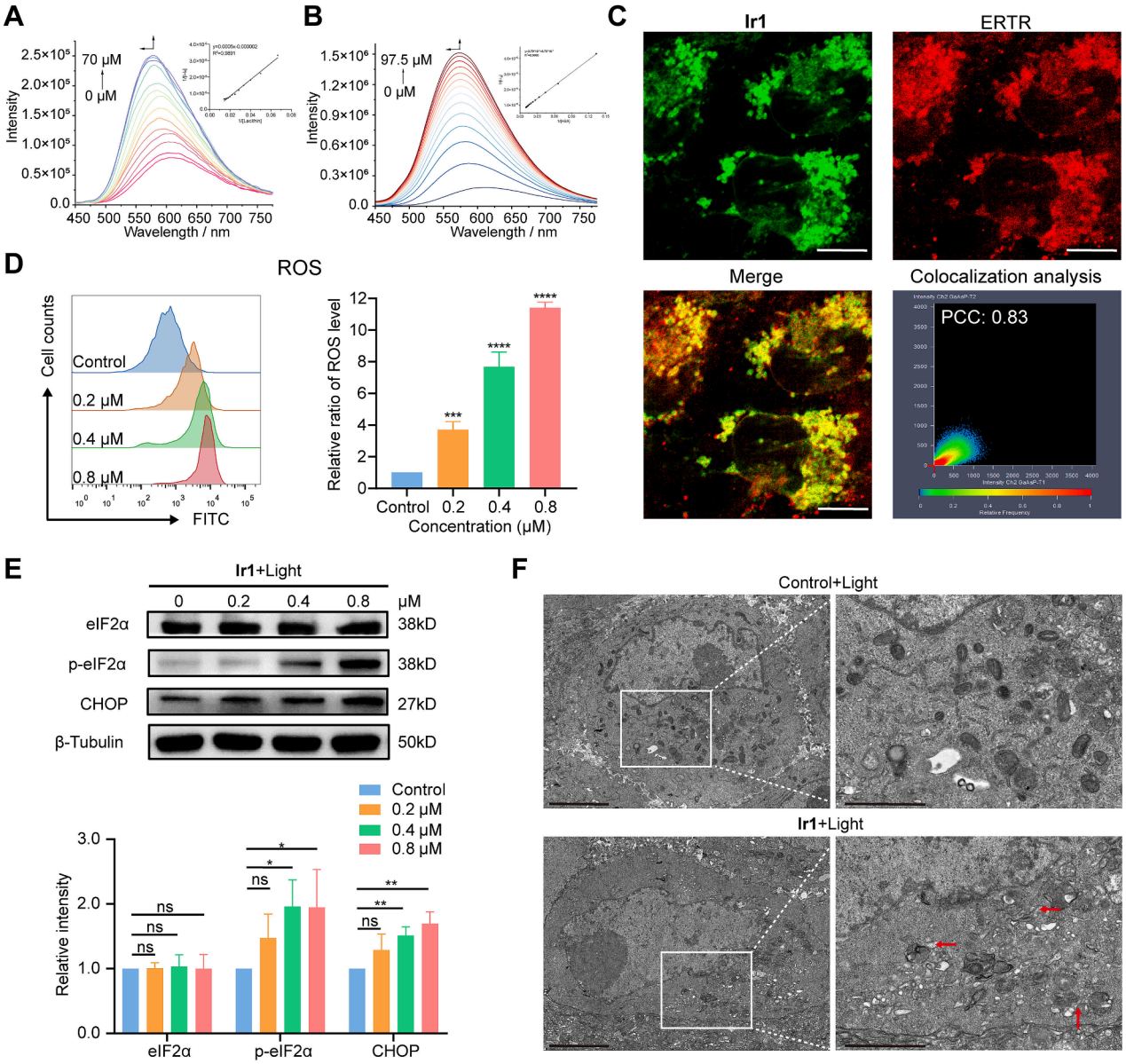

Fig. 2. **Ir1** selectively targets ER and elicits ROS-induced ER stress upon PDT *in vitro*. (A) Emission spectra of **Ir1** (10 μM) titrated with lecithin (0–70 μM) in Tris-HCl buffer. Inset: The Benesi–Hildebrand plot of $1/[I_{(600\ nm)}–I_{0(600\ nm)}]$ against 1/[lecithin]. λ_{ex} = 405 nm. (B) Emission spectra of **Ir1** (10 μM) titrated with HSA (0–97.5 μM) in Tris-HCl buffer. Inset: The Benesi–Hildebrand plot of $1/[I_{(600\ nm)}–I_{0(600\ nm)}]$ against 1/[HSA]. λ_{ex} = 405 nm. (C) Confocal spectroscopic observation of co-localization of **Ir1** (10 μM, 30 min) with ERTR (1 μM, 15 min) in SCC1 cells. **Ir1**: λ_{ex} = 405 nm; λ_{em} = 620 ± 20 nm. ERTR: λ_{ex} = 561 nm; λ_{em} = 610 ± 20 nm. Scale bars: 10 μm. (D) Intracellular ROS levels measured by DCFH-DA staining via flow cytometry. SCC1 cells were incubated with **Ir1** for 24 h and irradiated with a 425 nm laser (20 mW cm^{-2}, 15 min) before incubating with DCFH-DA (10 μM, 20 min). DCF: λ_{ex} = 488 nm, λ_{em} = 525 ± 20 nm. (E) The impact of **Ir1**-mediated PDT on the expression of eIF2α, p-eIF2α and CHOP by western blotting in SCC1 cells. Quantitative analysis of western blotting of three independent repeats was performed by ImageJ software. (F) TEM images of cell morphology upon PDT treatment by **Ir1** (0.8 μM, 24 h) in the presence of a 425 nm laser (20 mW cm^{-2}, 15 min). Scale bars: 5 μm and 2 μm. In panel D and E, data were shown as the mean ± SD of three biological replicates; ns, no significance; $^{*}p < 0.05$, $^{**}p < 0.01$, $^{***}p < 0.001$ and $^{****}p < 0.0001$.

on all the cancer cell lines. Upon irradiation at 425 nm, **Ir1** and **Ir2** show potent photocytotoxicity. Generally, the phototoxicity of **Ir1** is higher than that of **Ir2**, which is consistent with its high capability to generate ROS *in vitro*. Among the tested OSCC cell lines, SCC1 cells show the highest sensitivity to the PDT treatment, and the photocytotoxicity index (PI) values of **Ir1** and **Ir2** in SCC1 cells are 120.43 and 43.66, respectively. In addition, the UV/Vis absorbance of iridium complexes is proportional to the concentration up to 100 μM (Fig. S17), which indicates that **Ir1** and **Ir2** can be completely dissolved at the working concentrations.

Due to the capability of **Ir1** to generate O_2-dependent $^1O_2$ and O_2-independent •OH, we also evaluated its PDT effects on cell lines under hypoxic conditions and 3D tumor spheroids simulating the hypoxic TME. The phototoxicity of **Ir1** is well maintained under hypoxia, and the PI values of **Ir1** on SCC1 and SCC7 (murine squamous cell carcinoma cell line) cells are 95.24 and 30.22, respectively (Table S3). Moreover, **Ir1**-treated SCC1 and SCC7 tumor spheroids in combination with light show significantly diminished fluorescence, indicating **Ir1** can penetrate the 3D cellular architecture to eradicate tumor cells under hypoxic condition (Fig. S18). These results show that **Ir1** can overcome the hypoxic TME by eliciting PDT through both type I and II pathways.

2.3. Ir1 selectively accumulates in ER and elicits ROS-induced ER stress upon PDT

The cellular uptake and subcellular localization of metal-based agents are important factors influencing the anticancer efficacies [38]. Firstly, cellular uptake mechanism of **Ir1** has been investigated using confocal laser scanning microscopy. Results indicate that tumor cells pretreated with energy inhibitor and endocytic inhibitor or at low temperature show suppressed cellular luminescence, suggesting that **Ir1** is uptaken by tumor cells mainly through an energy-dependent endocytosis pathway (Fig. S19).

The long carbon chain and benzene ring at the end of the ligand in our molecules are hydrophobic, which would be embedded into the "non-polar tail" of phospholipid or hydrophobic cavities of protein. ER is the largest organelle of the cell involved in lipid and protein synthesis [39]. To verify our molecular design, we studied the binding of **Ir1** towards lecithin (the prominent phospholipid of ER membrane) and human serum albumin (HSA) as a model protein [40]. The emission intensity of **Ir1** increases by 3-fold in the presence of lecithin accompanied by a slight blueshift in the emission maxima, and the Benesi–Hildebrand binding constants (K_b) of **Ir1** towards lecithin is calculated to be 1.6×10^4 M^{-1} (Fig. 2A). Similarly, the titration results of **Ir1** on HSA show that the emission intensity increases by almost 7-fold in the presence of HSA and the K_b of **Ir1** towards HSA is calculated to be 3.06×10^4 M^{-1} (Fig. 2B). Colocalization assay using the commercial subcellular organelle-specific staining probes shows that **Ir1** can well colocalize with ER-Tracker Red (ERTR) with a high Pearson's correlation coefficient (PCC: 0.83 ± 0.01; Fig. 2C), while it shows minimal colocalization with MitoTracker Deep Red (MTDR, PCC: 0.31 ± 0.04) and LysoTracker Deep Red (LTDR, PCC: 0.44 ± 0.05; Fig. S20). These results indicate that **Ir1** can target ER possibly by binding with the phospholipids and proteins.

We then assessed the capability of **Ir1** to produce ROS upon light irradiation using 2′,7′-dichlorodihydrofluorescein diacetate (DCFH-DA) staining, which can be oxidized to highly emissive 2′,7′-dichlorodihydrofluorescein (DCF) by cellular ROS. A dose-dependent increase in DCF fluorescence is observed upon **Ir1**-mediated PDT treatment. **Ir1** elevates the cellular ROS level to about 11.7-fold at 0.8 μM in the presence of light (Fig. 2D).

Moreover, cells subjected to **Ir1**-mediated PDT at different concentrations were tested by western blotting for the two ER stress related proteins, eukaryotic initiation factor 2 alpha (eIF2α) and C/EBP homologous protein (CHOP) [41,42]. Upon PDT treatment with **Ir1**, CHOP and phosphorylation of eIF2α (p-eIF2α) are upregulated (Fig. 2E). These results indicate that **Ir1**-mediated PDT induces ER stress via eIF2α-dependent canonical pathway.

Finally, the alterations in cell morphology upon **Ir1** treatment were observed by transmission electron microscopy (TEM). Compared with the control, cells treated with **Ir1** (0.8 μM, 24 h) in combination with light show typical ultrastructural characteristics of disrupted morphology including ER swelling and vacuolization (Fig. 2F).

2.4. Ir1-mediated PDT triggers ICD and adaptively upregulates PD-L1 expression in vitro

ER stress is considered to be a prominent factor in the induction of ICD [18,43]. Therefore, we investigated the ability of **Ir1** to induce ICD *in vitro*. ICD can initiate immune response by the expression of DAMPs in dying tumor cells charactering with calreticulin (CRT) exposure, high mobility group box-1 protein (HMGB1) migration and adenosine triphosphate (ATP) secretion to achieve a long-term anticancer effect [44]. Flow cytometric results show an obvious concentration-dependent increase of CRT on cell surface upon **Ir1**-mediated PDT treatment (Fig. 3A). Meanwhile, cells with PDT treatment show apparent decrease of nuclear HMGB1, indicating the migration of HMGB1 from the nucleus to the extracellular region after treatment (Fig. 3B). Additionally, a dose-dependent increase in the content of extracellular ATP is also detected by chemiluminescence assay upon **Ir1**-mediated PDT treatment (Fig. 3C). However, both cisplatin and oxaliplatin fail to induce robust ICD in OSCC cells (Fig. S21).

Bioinformatic analysis indicates that CRT is significantly positively correlated with PD-L1 expression in OSCC patients, which inspires us to inquire whether **Ir1** could promote the increase of PD-L1 (Fig. 3D). Surprisingly, upon **Ir1**-mediated PDT treatment, PD-L1 expression is upregulated in a concentration-dependent manner by both real-time quantitative polymerase chain reaction (RT-qPCR; Fig. 3E) and western blotting (Fig. 3F). HSF1–HSP90 axis, NF-κB and YAP1 signaling pathways may enhance the functional expression of PD-L1 after treatment with metallo-anticancer agents [45–47]. However, the exact mechanism of PD-L1 upregulation by ICD inducers remains unclear and needs to be further explored. These results show that **Ir1**-mediated PDT can induce ROS-based ER stress to initiate ICD and adaptively upregulates PD-L1 expression.

2.5. Ir1-mediated PDT in combination with PD-L1 inhibitor inhibits oral carcinogenesis in 4NQO induced rat model

As **Ir1**-mediated PDT upregulates the expression of PD-L1 on tumor cells *in vitro*, which inspires us to propose the combination of PDT and PD-L1 inhibitor for synergistic antitumor effects. Oral carcinogenesis is a multistep evolutionary process from hyperplasia to dysplasia then carcinoma in situ and finally invasive carcinoma, which provides a window of opportunity for intervention [48]. BMS-1 is one of the small molecule agents that can induce PD-L1 dimerization and thereby block the interaction with PD-1, which possesses many advantages such as ease of synthesis, high stability, improved tumor penetration, and low costs compared with monoclonal antibody [49,50]. The schematic illustration of establishment and experimental procedure for 4NQO induced oral carcinogenesis rat model is shown in Fig. 4A. After the 16-week carcinogen treatment, the lesions exhibit white masses with a wrinkled paper-like or verrucous appearance, indicating the successful establishment of model to implement intervention. Upon accomplishing intervention with certain treatment, the lesions in control group develop into rough and hard surfaces accompanied by erosion, ulcer and endogenous growth with unclear boundaries, while the malignancy in combination treatment group turns out to be inhibited (Fig. 4B and S22).

Then, a histopathologic assessment of rat tongue samples was performed based on the hematoxylin eosin (H&E) staining. In the combination treatment group, only 1 (20%) case develops into mild invasion carcinoma, while in control group, 2 (40%) cases develop into moderate

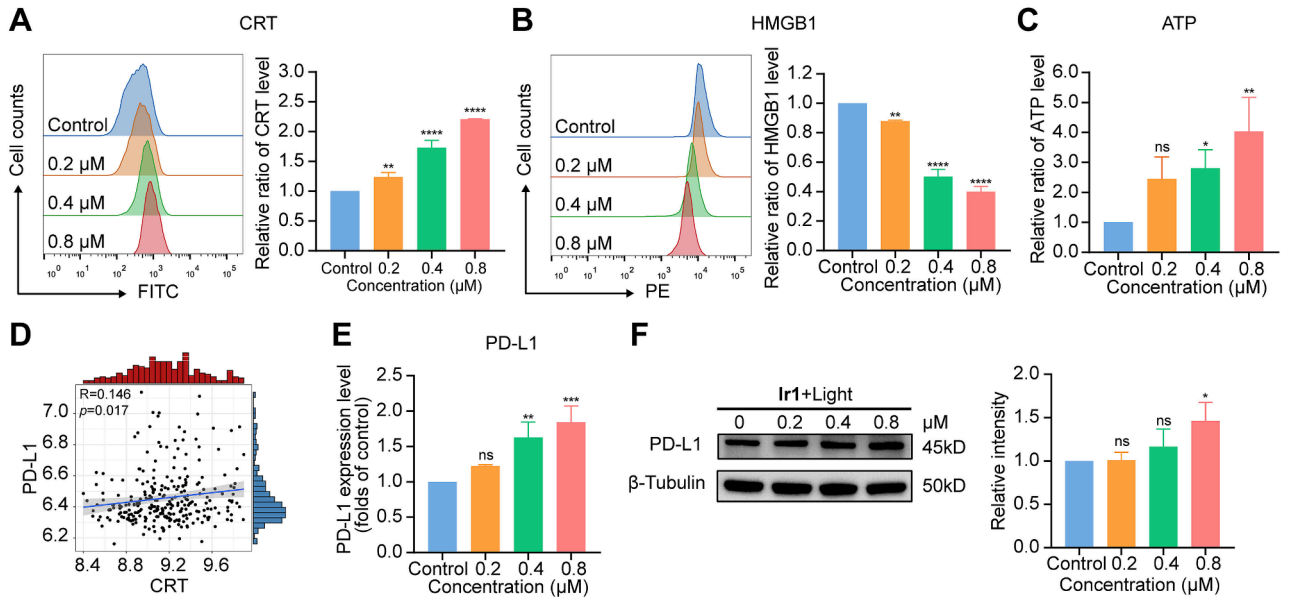

Fig. 3. **Ir1**-mediated PDT triggers ICD and adaptively upregulates PD-L1 expression *in vitro*. (A-B) Cell surface CRT (A) and nuclear HMGB1 (B) expression levels in **Ir1**-treated SCC1 cells measured by flow cytometry. SCC1 cells were incubated with **Ir1** (0.2, 0.4 and 0.8 μM) for 24 h and irradiated with a 425 nm laser (20 mW cm^{-2}, 15 min). (C) Extracellular ATP levels in **Ir1**-treated SCC1 cells measured by chemiluminescence assay. SCC1 cells were incubated with **Ir1** for 24 h and irradiated with a 425 nm laser (20 mW cm^{-2}, 15 min). (D) Correlation analysis between CRT and PD-L1 of OSCC patients in GSE65858 dataset. (E-F) The expression of PD-L1 in SCC1 cells treated with **Ir1** (0.2, 0.4 and 0.8 μM; 24 h) in the presence of light (425 nm, 20 mW cm^{-2}, 15 min) was measured by RT-qPCR (E) and western blotting (F). Quantitative analysis of western blotting of three independent repeats was performed by ImageJ software. In panel A-C and E-F, data were shown as the mean ± SD of three biological replicates; ns, no significance; $^{*}p < 0.05$, $^{**}p < 0.01$, $^{***}p < 0.001$ and $^{****}p < 0.0001$.

invasion carcinoma and 3 (60%) cases develop into severe invasion carcinoma in their tongues (Fig. 4C and Table S4). Monotherapy with either **Ir1**-mediated PDT or PD-L1 inhibitor interrupts the malignant transformation process, while no significant inhibition is found in **Ir1** group without light irradiation (Fig. 4C and Table S4). Additionally, the combination treatment group possesses the strongest inhibition effect with the mean H&E score of 4, which is significantly lower than that in the control group (H&E score = 7.6; $p < 0.001$; Fig. 4D).

Immunohistochemistry (IHC) results show that **Ir1**-mediated PDT in combination with PD-L1 inhibitor significantly decreases the positive rates of Ki67. Meanwhile, the number of $PD\text{-}L1^{+}$ cells is significantly increased in the **Ir1**-mediated PDT group, while the immunosuppression status is attenuated by PD-L1 inhibitor treatment (Fig. 4E). Taken together, these results indicate that the **Ir1**-mediated PDT exhibits significant carcinogenesis inhibition effects and synergizes with PD-L1 therapy in 4NQO induced rat model.

2.6. *Ir1-mediated PDT enhances the antitumor efficacy in combination with PD-L1 inhibitor in vivo*

The antitumor efficacy was further evaluated in C57BL/6 mice bearing SCC7 tumors (Fig. 5A). Both **Ir1**-medidated PDT and PD-L1 inhibitor show a remarkable inhibition on tumor growth, and the combination of the two modalities more significantly achieves the regression of tumors (Fig. 5B). Meanwhile, no significant weight change is found during treatment process, suggesting the relative safety for administration (Fig. S23). Subsequently, the tumor tissues from each group were harvested. The average tumor weight of mice treated with saline, **Ir1** + light, PD-L1 inhibitor, and combination treatment is 0.46 g, 0.19 g, 0.19 g, and 0.10 g respectively, indicating **Ir1**-mediated PDT plus PD-L1 inhibitor possesses the best antitumor effect (Fig. 5C and D).

To further validate the therapeutic effects, H&E and IHC staining were performed on tumor tissue slices. In the combination treatment group, H&E staining shows severe necrosis with noticeable vacuolization, massive nucleus absence and conspicuous karyopyknosis, revealing the efficient antitumor killing effects (Fig. 5E). No serious structural or pathological alterations in major organs (heart, liver, spleen, lung and kidney) are found in all the treatment groups according to the histochemical analysis, indicating the low systemic toxicity of treatments (Fig. S24). Moreover, IHC staining shows that the expression of Ki67 is significantly decreased in **Ir1**-medidated PDT and combination treatment mice, exerting a strong inhibition on tumor cell proliferation. Notability, the PD-L1 expression is significantly upregulated in **Ir1**-medidated PDT group, which is consistent with the *in vitro* study, further proving the feasibility of combination therapy. Encouragingly, in the combination treatment group, **Ir1**-mediated high PD-L1 expression is reversed by the PD-L1 inhibitor to attenuate the immunosuppression (Fig. 5E). Taken together, these results indicate that **Ir1**-medidated PDT plus PD-L1 inhibitor has the strongest tumor suppressive effect and relieves the immunosuppressive TME *in vivo*.

2.7. *Ir1-medidated PDT combined with PD-L1 inhibitor synergistically augments antitumor immune responses*

In order to investigate the potential immune mechanisms related to the favorable *in vivo* performance of combination treatment, a series of immune studies were performed. CRT serves as an important “eat me” signal, which could help to promote tumor-specific antigen recognition and presentation and induce DCs maturation [51]. Compared with the control group, the proportion of CRT^{+} tumor cells increases by about 2-fold in the **Ir1**-mediated PDT and combination treatment groups, verifying that **Ir1**-mediated PDT triggers ICD (Fig. 6A).

To further determine if **Ir1**-mediated ICD alters the phenotypic and functional maturation of DCs, the major histocompatibility class II (MHC-II) and costimulatory molecule CD80/CD86 on the surface of DCs were analyzed by flow cytometry. As shown in Fig. 6B and 6C, the combination of PDT with PD-L1 inhibitor significantly upregulates the contents of $MHC\ II^{+}$ and $CD80^{+}CD86^{+}$ DCs, which is superior to monotherapy with either ICD induction or PD-L1 inhibition.

Mature DCs can present antigens to T cells, thereby activating T cells in TME to elicit adaptive immune responses [52,53]. Compared with the control and monotherapy groups, the combination treatment increases a

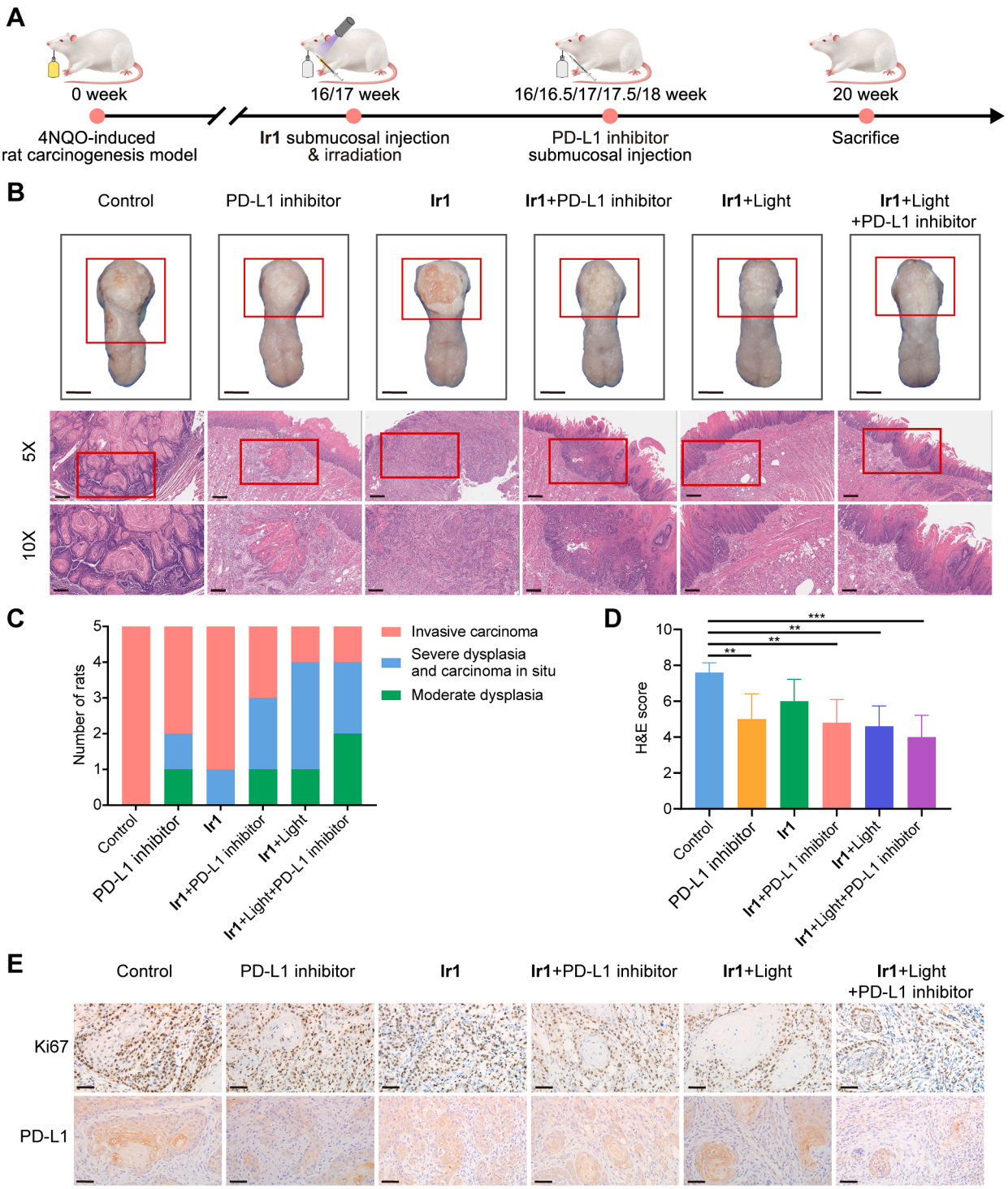

Fig. 4. **Ir1**-mediated PDT in combination with PD-L1 inhibitor inhibits carcinogenesis in 4NQO induced rat model. (A) Schematic overview of the 4NQO model experimental design. (B) Representative gross observation and H&E images of the rat tongues in different groups at the endpoint. Scale bars: 5 mm for gross observation, 400 μm for 5 × magnification and 200 μm for 10 × magnification. (C) Quantification of the histological degree of moderate dysplasia, severe dysplasia and carcinoma in situ, and invasive carcinoma in the six groups. (D) H&E scores of the histopathologic diagnoses in the six groups. (E) Representative IHC staining of Ki67 and PD-L1. Scale bars: 50 μm. In panel D, data were shown as the mean ± SD. $^{**}p < 0.01$ and $^{***}p < 0.001$.

high level of tumor-specific $CD4^+$ and $CD8^+$ T cell infiltration, indicating **Ir1**-mediated PDT and PD-L1 inhibitor treatment act synergistically to potentiate anti-tumor adaptive immunity (Fig. 6D and E). It is also noteworthy that the PDT-induced increase of PD-1 expression on $CD8^+$ T cells is reversed by the PD-L1 inhibition (Fig. 6F).

Subsequently, cytokines including tumor necrosis factor-α (TNF-α), interferon-γ (IFN-γ) and interleukin-6 (IL-6) in tumors were analyzed by enzyme-linked immunosorbent assay (ELISA). Consistent with above findings, the amount of TNF-α and IFN-γ in tumors also appears to be the highest in the combination therapy group for the activation of antitumor immunity (Fig. 6G). Meanwhile, immunosuppressive inflammatory cytokine IL-6 is remarkably downregulated after combination treatment as compared to control group (Fig. 6G). TNF-α and IFN-γ are key regulators for killing tumor and boosting antitumor immune response in the

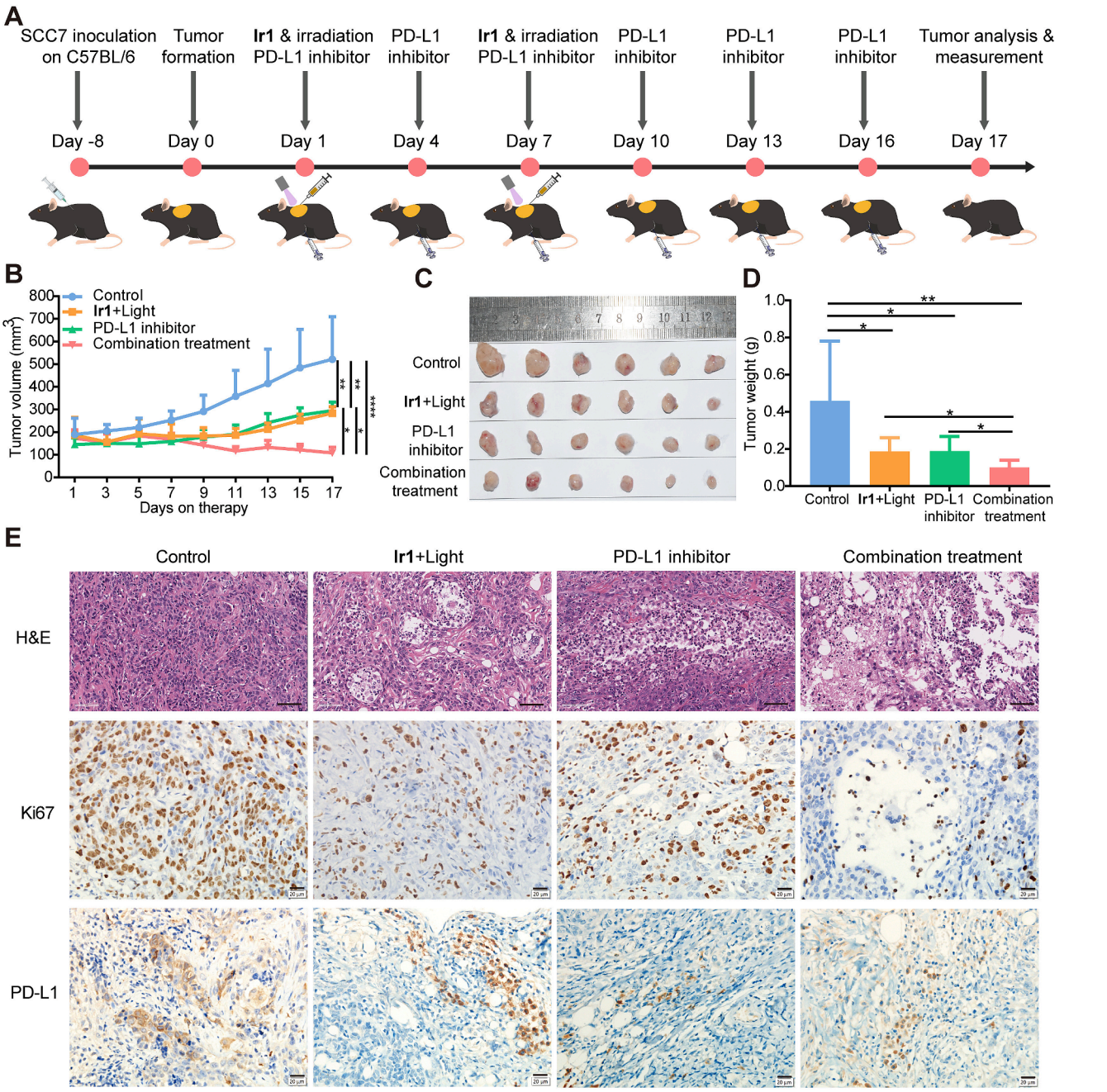

Fig. 5. **Ir1**-mediated PDT in combination with PD-L1 inhibitor exhibits potent antitumor effects in CDX model. (A) Timeline illustration of the SCC7 xenograft model establishment and therapeutic process in C57BL/6 mice. (B) Tumor growth curves of mice with indicated treatments for 17 days. (C) Representative images of the resected tumors at the end of the treatment. (D) The tumor weight at the end of the treatment. (E) H&E and IHC staining for Ki67 and PD-L1 of tumor sections after various treatments. Scale bar: 60 μm for H&E and 20 μm for IHC. In panel B and D, data were shown as the mean ± SD. *$p < 0.05$, **$p < 0.01$ and ****$p < 0.0001$.

TME [54,55]. We find patients with higher expression of TNF-α and IFN-γ have longer overall survival than those with low expression in TCGA dataset (Fig. 6H). IL–6 signaling acts to drive the proliferation, invasiveness and metastasis of tumor cells, and prevents T cell activation to suppresses the antitumor immune response [56]. High expression of IL-6 is also associated with a poor clinical prognosis in GSE4163 dataset (Fig. 6H). Besides, the correlation between CRT and resting DCs was further analyzed in TCGA dataset. The result reveals that CRT is significantly negatively correlated with resting DCs in tumor tissues, suggesting the resting DCs have been activated with the increase of CRT (Fig. S25). These results collectively show that the combination of **Ir1**-mediated PDT with PD-L1 blockade facilitates the maturation of DCs, enhances the recruitment and activation of antitumor T cells, promotes the secretion of multiple antitumor cytokines and improves the response rate of PD-L1 inhibitor, which transforms "cold tumor" into "hot tumor" for synergetic immunotherapy.

3. Conclusion

In this study, we designed two new iridium(III) photosensitizers incorporating a ligand targeting ER by interacting with phospholipids and proteins. **Ir1** can generate ROS through both type I/II PDT pathways to elicit ER stress in OSCC tumor cells upon irradiation. Interestingly, PDT treatment generates ICD leading to the release of DAMPs, which promotes the upregulation of PD-L1 expression, yielding a basis on the synergistic therapy. We prove that **Ir1**-mediated PDT induces the

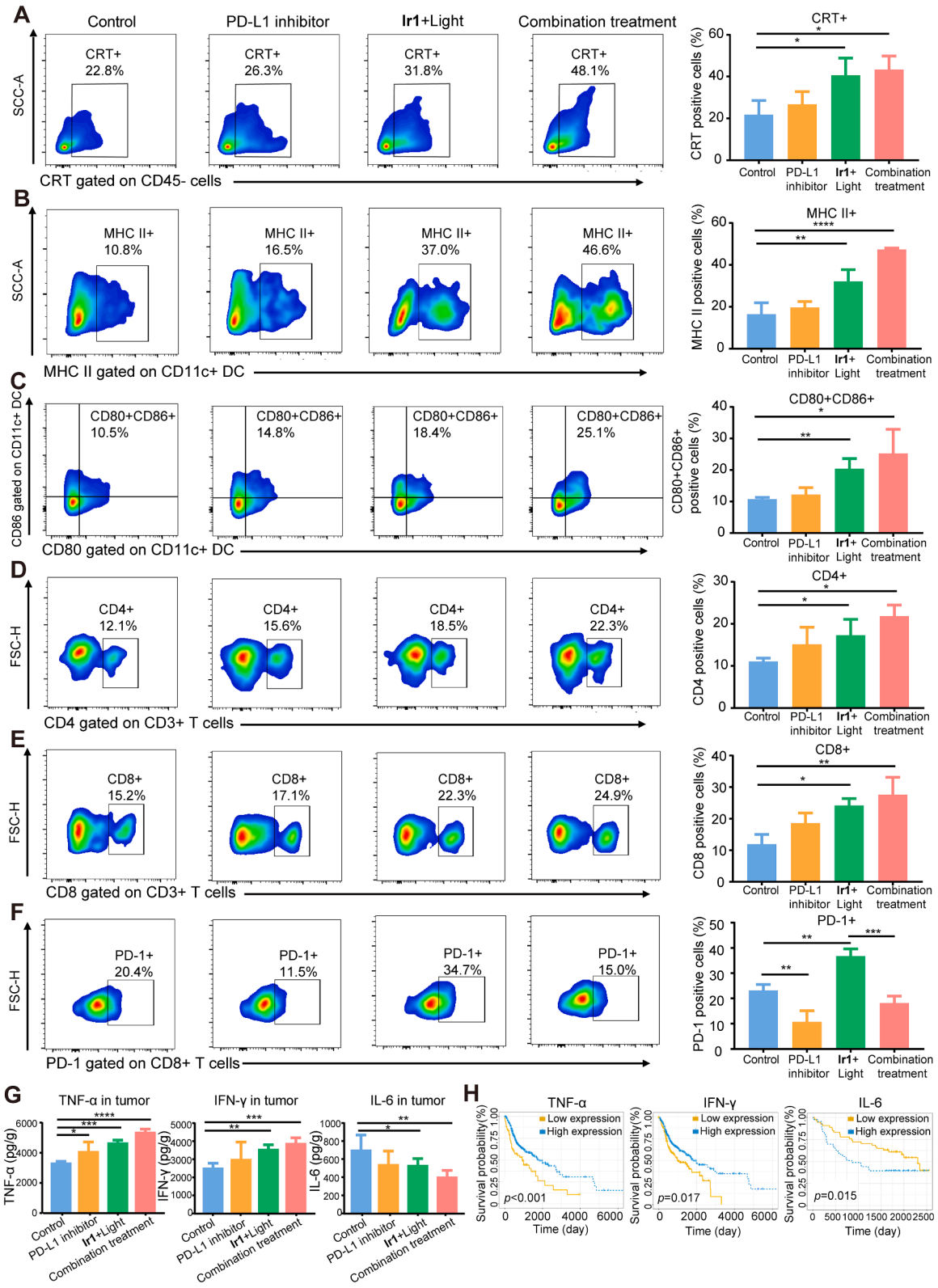

Fig. 6. **Ir1**-mediated PDT enhances the immunogenicity and sensitizes tumors to PD-L1 inhibitor for potent anticancer immunity in CDX model. (A) Representative flow cytometry dot plots and statistical analysis of CRT expression (CRT^+ cells gated on $CD45^-$) on tumor cell surface after various treatments. (B-C) Representative flow cytometry dot plots and statistical analysis of activated DCs ($MHC\ II^+$ cells gated on $CD45^+CD11c^+$; B) and mature DCs ($CD80^+CD86^+$ cells gated on $CD45^+CD11c^+$; C) in tumors. (D-E) Representative flow cytometry dot plots and statistical analysis of $CD4^+$ T cells ($CD4^+$ cells gated on $CD45^+CD3^+$; D) and $CD8^+$ T cells ($CD8^+$ cells gated on $CD45^+CD3^+$; E) infiltration in tumors after various treatments. (F) Representative flow cytometry dot plots and statistical analysis of $PD\text{-}1^+$ T cells ($PD\text{-}1^+$ cells gated on $CD45^+CD3^+CD8^+$) infiltration in tumors after various treatments. (G) Levels of TNF-α, IFN-γ and IL-6 in tumor tissues of different treatment groups measured by ELISA. (H) Kaplan-Meier survival curves of overall survival based on OSCC patients with high- and low-expression of TNF-α, IFN-γ and IL-6 (TCGA and GSE41613). In panel A-G, data were shown as the mean ± SD. $*p < 0.05$, $**p < 0.01$, $***p < 0.001$ and $****p < 0.0001$.

maturation of DCs, promotes the infiltration and activation of T cells in TME, and synergizes with PD-L1 inhibitor to transform immune-suppressive "cold tumor" to immune-responsive "hot tumor" in both CDX and rat experimental carcinogenesis models. In summary, we firstly provide evidence for combining metal-based ICD-inducing photosensitizer with PD-L1 inhibitor to synergistically induce antitumor immune-responses, which offers a novel paradigm for OSCC treatment.

CRediT authorship contribution statement

Jia-Ying Zhou: Conceptualization, Methodology, Formal analysis, Investigation, Validation, Writing – original draft. **Qing-Hua Shen:** Conceptualization, Methodology, Formal analysis, Software, Writing – original draft. **Xiao-Jing Hong:** Methodology, Formal analysis, Software, Validation, Writing – original draft. **Wu-Ya Zhang:** Visualization, Software. **Qiao Su:** Methodology, Validation. **Wu-Guo Li:** Methodology, Validation. **Bin Cheng:** Validation, Supervision, Funding acquisition. **Cai-Ping Tan:** Conceptualization, Supervision, Funding acquisition, Writing – review & editing. **Tong Wu:** Conceptualization, Validation, Supervision, Writing – review & editing.

Declaration of Competing Interest

The authors declare that they have no known competing financial interests or personal relationships that could have appeared to influence the work reported in this paper.

Data availability

Data will be made available on request.

Acknowledgements

Jia-Ying Zhou, Qing-Hua Shen and Xiao-Jing Hong contributed equally to this work. This study was supported by the Science and Technology Project of Guangzhou, China (Grant No. 202206080009) and the National Natural Science Foundation of China (Nos. 22022707 and 22177142). Scheme 1C was created with biorender.com.

Appendix A. Supplementary data

Supplementary data to this article can be found online at https://doi.org/10.1016/j.cej.2023.145516.

References

[1] X. Li, J.F. Lovell, J. Yoon, X. Chen, Clinical development and potential of photothermal and photodynamic therapies for cancer, Nat. Rev. Clin. Oncol. 17 (11) (2020) 657–674.
[2] R. Alzeibak, T.A. Mishchenko, N.Y. Shilyagina, I.V. Balalaeva, M.V. Vedunova, D. V. Krysko, Targeting immunogenic cancer cell death by photodynamic therapy: past, present and future, J. Immunother. Cancer 9 (1) (2021), e001926.
[3] D.V. Krysko, A.D. Garg, A. Kaczmarek, O. Krysko, P. Agostinis, P. Vandenabeele, Immunogenic cell death and DAMPs in cancer therapy, Nat. Rev. Cancer 12 (12) (2012) 860–875.
[4] G. Kroemer, C. Galassi, L. Zitvogel, L. Galluzzi, Immunogenic cell stress and death, Nat. Immunol. 23 (4) (2022) 487–500.
[5] C. Zhang, C. Xu, X. Gao, Q. Yao, Platinum-based drugs for cancer therapy and anti-tumor strategies, Theranostics 12 (5) (2022) 2115–2132.
[6] S.J. Park, W. Ye, R. Xiao, C. Silvin, M. Padget, J.W. Hodge, C. Van Waes, N. C. Schmitt, Cisplatin and oxaliplatin induce similar immunogenic changes in preclinical models of head and neck cancer, Oral Oncol. 95 (2019) 127–135.
[7] G. He, M. He, R. Wang, X. Li, H. Hu, D. Wang, Z. Wang, Y. Lu, N. Xu, J. Du, J. Fan, X. Peng, W. Sun, A near-infrared light-activated photocage based on a ruthenium complex for cancer phototherapy, Angew. Chem. Int. Ed. Engl. 62 (24) (2023), e202218768.
[8] X.Q. Zhou, P. Wang, V. Ramu, L. Zhang, S. Jiang, X. Li, S. Abyar, P. Papadopoulou, Y. Shao, L. Bretin, M.A. Siegler, F. Buda, A. Kros, J. Fan, X. Peng, W. Sun, S. Bonnet, In vivo metallophilic self-assembly of a light-activated anticancer drug, Nat. Chem. 15 (7) (2023) 980–987.
[9] S. Sen, M. Won, M.S. Levine, Y. Noh, A.C. Sedgwick, J.S. Kim, J.L. Sessler, J. F. Arambula, Metal-based anticancer agents as immunogenic cell death inducers: the past, present, and future, Chem. Soc. Rev. 51 (4) (2022) 1212–1233.
[10] L. Zhang, N. Montesdeoca, J. Karges, H. Xiao, Immunogenic cell death inducing metal complexes for cancer therapy, Angew. Chem. Int. Ed. Engl. (2023), e202300662.
[11] J. Karges, Clinical development of metal complexes as photosensitizers for photodynamic therapy of cancer, Angew. Chem. Int. Ed. Engl. 61 (5) (2022), e202112236.
[12] L. Wang, R. Guan, L. Xie, X. Liao, K. Xiong, T.W. Rees, Y. Chen, L. Ji, H. Chao, An ER-targeting iridium(III) complex that induces immunogenic cell death in non-small-cell lung cancer, Angew. Chem. Int. Ed. Engl. 60 (9) (2021) 4657–4665.
[13] H. Yuan, Z. Han, Y. Chen, F. Qi, H. Fang, Z. Guo, S. Zhang, W. He, Ferroptosis photoinduced by new cyclometalated iridium(III) complexes and its synergism with apoptosis in tumor cell inhibition, Angew. Chem. Int. Ed. Engl. 60 (15) (2021) 8174–8181.
[14] L. He, Y. Li, C.P. Tan, R.R. Ye, M.H. Chen, J.J. Cao, L.N. Ji, Z.W. Mao, Cyclometalated iridium(iii) complexes as lysosome-targeted photodynamic anticancer and real-time tracking agents, Chem. Sci. 6 (10) (2015) 5409–5418.
[15] J.S. Nam, M.G. Kang, J. Kang, S.Y. Park, S.J. Lee, H.T. Kim, J.K. Seo, O.H. Kwon, M. H. Lim, H.W. Rhee, T.H. Kwon, Endoplasmic reticulum-localized iridium(III) complexes as efficient photodynamic therapy agents via protein modifications, J. Am. Chem. Soc. 138 (34) (2016) 10968–10977.
[16] R. Bevernaegie, B. Doix, E. Bastien, A. Diman, A. Decottignies, O. Feron, B. Elias, Exploring the phototoxicity of hypoxic active iridium(III)-based sensitizers in 3D tumor spheroids, J. Am. Chem. Soc. 141 (46) (2019) 18486–18491.
[17] D.S. Schwarz, M.D. Blower, The endoplasmic reticulum: structure, function and response to cellular signaling, Cell. Mol. Life Sci. 73 (1) (2016) 79–94.
[18] W. Li, J. Yang, L. Luo, M. Jiang, B. Qin, H. Yin, C. Zhu, X. Yuan, J. Zhang, Z. Luo, Y. Du, Q. Li, Y. Lou, Y. Qiu, J. You, Targeting photodynamic and photothermal therapy to the endoplasmic reticulum enhances immunogenic cancer cell death, Nat. Commun. 10 (1) (2019) 3349.
[19] A.P. King, J.J. Wilson, Endoplasmic reticulum stress: an arising target for metal-based anticancer agents, Chem. Soc. Rev. 49 (22) (2020) 8113–8136.
[20] N. Rufo, A.D. Garg, P. Agostinis, The unfolded protein response in immunogenic cell death and cancer immunotherapy, Trends Cancer 3 (9) (2017) 643–658.
[21] K. Xiong, F. Wei, Y. Chen, L. Ji, H. Chao, Recent progress in photodynamic immunotherapy with metal-based photosensitizers, Small Methods 7 (5) (2022) e2201403.
[22] Y.Y. Ling, W.J. Wang, L. Hao, X.W. Wu, J.H. Liang, H. Zhang, Z.W. Mao, C.P. Tan, Self-amplifying iridium(III) photosensitizer for ferroptosis-mediated immunotherapy against transferrin receptor-overexpressing cancer, Small 18 (49) (2022) e2203659.
[23] L. Zhou, F. Wei, J. Xiang, H. Li, C. Li, P. Zhang, C. Liu, P. Gong, L. Cai, K.M. Wong, Enhancing the ROS generation ability of a rhodamine-decorated iridium(iii) complex by ligand regulation for endoplasmic reticulum-targeted photodynamic therapy, Chem. Sci. 11 (44) (2020) 12212–12220.
[24] L. Fournel, Z. Wu, N. Stadler, D. Damotte, F. Lococo, G. Boulle, E. Segal-Bendirdjian, A. Bobbio, P. Icard, J. Tredaniel, M. Alifano, P. Forgez, Cisplatin increases PD-L1 expression and optimizes immune check-point blockade in non-small cell lung cancer, Cancer Lett. 464 (2019) 5–14.
[25] L. Li, Y. Li, C.H. Yang, D.C. Radford, J. Wang, M. Janat-Amsbury, J. Kopecek, J. Yang, Inhibition of immunosuppressive tumors by polymer-assisted inductions of immunogenic cell death and multivalent PD-L1 crosslinking, Adv. Funct. Mater. 30 (12) (2020), 1908961.
[26] M. Wu, Q. Huang, Y. Xie, X. Wu, H. Ma, Y. Zhang, Y. Xia, Improvement of the anticancer efficacy of PD-1/PD-L1 blockade via combination therapy and PD-L1 regulation, J. Hematol. Oncol. 15 (1) (2022) 24.
[27] B. Zhao, H. Zhao, J. Zhao, Efficacy of PD-1/PD-L1 blockade monotherapy in clinical trials, Ther. Adv. Med. Oncol. 12 (2020) 1758835920937612.
[28] O. Kujan, B. van Schaijik, C.S. Farah, Immune checkpoint inhibitors in oral cavity squamous cell carcinoma and oral potentially malignant disorders: a systematic review, Cancers (Basel) 12 (7) (2020) 1937.
[29] J. Galon, D. Bruni, Approaches to treat immune hot, altered and cold tumours with combination immunotherapies, Nat. Rev. Drug Discov. 18 (3) (2019) 197–218.
[30] J. Haanen, Converting cold into hot tumors by combining immunotherapies, Cell 170 (6) (2017) 1055–1056.
[31] O. Kepp, L. Zitvogel, G. Kroemer, Clinical evidence that immunogenic cell death sensitizes to PD-1/PD-L1 blockade, Oncoimmunology 8 (10) (2019), e1637188.
[32] S. Yin, Z. Chen, D. Chen, D. Yan, Strategies targeting PD-L1 expression and associated opportunities for cancer combination therapy, Theranostics 13 (5) (2023) 1520–1544.
[33] C.J. Langer, S.M. Gadgeel, H. Borghaei, V.A. Papadimitrakopoulou, A. Patnaik, S. F. Powell, R.D. Gentzler, R.G. Martins, J.P. Stevenson, S.I. Jalal, A. Panwalkar, J. C. Yang, M. Gubens, L.V. Sequist, M.M. Awad, J. Fiore, Y. Ge, H. Raftopoulos, L. Gandhi, Carboplatin and pemetrexed with or without pembrolizumab for advanced, non-squamous non-small-cell lung cancer: a randomised, phase 2 cohort of the open-label KEYNOTE-021 study, Lancet Oncol. 17 (11) (2016) 1497–1508.
[34] S.K. Jabbour, A.T. Berman, R.H. Decker, Y. Lin, S.J. Feigenberg, S.N. Gettinger, C. Aggarwal, C.J. Langer, C.B. Simone 2nd, J.D. Bradley, J. Aisner, J. Malhotra, Phase 1 trial of Pembrolizumab administered concurrently with chemoradiotherapy for locally advanced non-small cell lung cancer: a nonrandomized controlled trial, JAMA Oncol. 6 (6) (2020) 848–855.
[35] K. Feng, Y. Liu, Y. Zhao, Q. Yang, L. Dong, J. Liu, X. Li, Z. Zhao, Q. Mei, W. Han, Efficacy and biomarker analysis of nivolumab plus gemcitabine and cisplatin in

patients with unresectable or metastatic biliary tract cancers: results from a phase II study, J. Immunother. Cancer 8 (1) (2020), e000367.
[36] J. Zhao, K. Yan, G. Xu, X. Liu, Q. Zhao, C. Xu, S. Gou, An iridium (III) complex bearing a donor–acceptor–donor type ligand for NIR-triggered dual phototherapy, Adv. Funct. Mater. 31 (11) (2021), 2008325.
[37] M. Kang, Z. Zhang, W. Xu, H. Wen, W. Zhu, Q. Wu, H. Wu, J. Gong, Z. Wang, D. Wang, B.Z. Tang, Good steel used in the blade: well-tailored type-I photosensitizers with aggregation-induced emission characteristics for precise nuclear targeting photodynamic therapy, Adv. Sci. 8 (14) (2021), e2100524.
[38] Y. Hui, X. Yi, F. Hou, D. Wibowo, F. Zhang, D. Zhao, H. Gao, C.X. Zhao, Role of nanoparticle mechanical properties in cancer drug delivery, ACS Nano 13 (7) (2019) 7410–7424.
[39] C. Celik, S.Y.T. Lee, W.S. Yap, G. Thibault, Endoplasmic reticulum stress and lipids in health and diseases, Prog. Lipid Res. 89 (2023), 101198.
[40] S. Zalba, T.L. Ten Hagen, Cell membrane modulation as adjuvant in cancer therapy, Cancer Treat. Rev. 52 (2017) 48–57.
[41] L. Bezu, A. Sauvat, J. Humeau, L.C. Gomes-da-Silva, K. Iribarren, S. Forveille, P. Garcia, L. Zhao, P. Liu, L. Zitvogel, L. Senovilla, O. Kepp, G. Kroemer, eIF2alpha phosphorylation is pathognomonic for immunogenic cell death, Cell Death Differ. 25 (8) (2018) 1375–1393.
[42] X. Chen, J.R. Cubillos-Ruiz, Endoplasmic reticulum stress signals in the tumour and its microenvironment, Nat. Rev. Cancer 21 (2) (2021) 71–88.
[43] H. Deng, Z. Zhou, W. Yang, L.S. Lin, S. Wang, G. Niu, J. Song, X. Chen, Endoplasmic reticulum targeting to amplify immunogenic cell death for cancer immunotherapy, Nano Lett. 20 (3) (2020) 1928–1933.
[44] Z. Li, X. Lai, S. Fu, L. Ren, H. Cai, H.u. Zhang, Z. Gu, X. Ma, K. Luo, Immunogenic cell death activates the tumor immune microenvironment to boost the immunotherapy efficiency, Adv. Sci. 9 (22) (2022), e2201734.
[45] T. Sasaya, T. Kubo, K. Murata, Y. Mizue, K. Sasaki, J. Yanagawa, M. Imagawa, H. Kato, T. Tsukahara, T. Kanaseki, Y. Tamura, A. Miyazaki, Y. Hirohashi, T. Torigoe, Cisplatin-induced HSF1-HSP90 axis enhances the expression of functional PD-L1 in oral squamous cell carcinoma, Cancer Med. 12 (4) (2023) 4605–4615.
[46] J. Peng, J. Hamanishi, N. Matsumura, K. Abiko, K. Murat, T. Baba, K. Yamaguchi, N. Horikawa, Y. Hosoe, S.K. Murphy, I. Konishi, M. Mandai, Chemotherapy induces programmed cell death-ligand 1 overexpression via the nuclear factor-kappaB to foster an immunosuppressive tumor microenvironment in ovarian cancer, Cancer Res. 75 (23) (2015) 5034–5045.
[47] S. Li, J. Ji, Z. Zhang, Q. Peng, L. Hao, Y. Guo, W. Zhou, Q. Cui, X. Shi, Cisplatin promotes the expression level of PD-L1 in the microenvironment of hepatocellular carcinoma through YAP1, Mol. Cell. Biochem. 475 (1–2) (2020) 79–91.
[48] D.E. Johnson, B. Burtness, C.R. Leemans, V.W.Y. Lui, J.E. Bauman, J.R. Grandis, Head and neck squamous cell carcinoma, Nat. Rev. Dis. Primers 6 (1) (2020) 92.
[49] T. Wang, X. Wu, C. Guo, K. Zhang, J. Xu, Z. Li, S. Jiang, Development of inhibitors of the programmed cell death-1/programmed cell death-ligand 1 signaling pathway, J. Med. Chem. 62 (4) (2019) 1715–1730.
[50] Q. Wu, L. Jiang, S.C. Li, Q.J. He, B. Yang, J. Cao, Small molecule inhibitors targeting the PD-1/PD-L1 signaling pathway, Acta Pharmacol. Sin. 42 (1) (2021) 1–9.
[51] J. Fucikova, R. Spisek, G. Kroemer, L. Galluzzi, Calreticulin and cancer, Cell Res. 31 (1) (2021) 5–16.
[52] S.K. Wculek, F.J. Cueto, A.M. Mujal, I. Melero, M.F. Krummel, D. Sancho, Dendritic cells in cancer immunology and immunotherapy, Nat. Rev. Immunol. 20 (1) (2020) 7–24.
[53] S. Jhunjhunwala, C. Hammer, L. Delamarre, Antigen presentation in cancer: insights into tumour immunogenicity and immune evasion, Nat. Rev. Cancer 21 (5) (2021) 298–312.
[54] J. Shen, Z. Xiao, Q. Zhao, M. Li, X. Wu, L. Zhang, W. Hu, C.H. Cho, Anti-cancer therapy with TNFalpha and IFNgamma: A comprehensive review, Cell Prolif. 51 (4) (2018) e12441.
[55] L.B. Ivashkiv, IFNgamma: signalling, epigenetics and roles in immunity, metabolism, disease and cancer immunotherapy, Nat. Rev. Immunol. 18 (9) (2018) 545–558.
[56] D.E. Johnson, R.A. O'Keefe, J.R. Grandis, Targeting the IL-6/JAK/STAT3 signalling axis in cancer, Nat. Rev. Clin. Oncol. 15 (4) (2018) 234–248.